Diffusion-weighted MRI beyond the central nervous system in children

Bilal Battal, Veysel Akgün, Murat Kocaoğlu

ABSTRACT
Diffusion-weighted imaging has recently been incorporated into extra-neurological pediatric imaging protocols because of its various clinical advantages. Because diffusion-weighted imaging does not require intravenous contrast media, it can be safely used in patients with reduced renal function. Furthermore, diffusion-weighted imaging can be performed within several minutes by using the echo planar imaging technique. Its clinical advantages include improved tissue characterization, as well as the ability to assess organ functionality, monitor the treatment response after chemotherapy or radiation therapy and predict patient outcomes. The aims of this pictorial essay were to explain the physical principles underlying diffusion-weighted imaging, to outline the interpretation of diffusion-weighted images and apparent diffusion coefficient maps, and to list the extra-neurological applications of diffusion-weighted imaging in children.

Key words: • diffusion-weighted MRI • tumor • pediatrics

From the Department of Radiology (B.B. ✉ *bilbat_23@yahoo.com*, M.K.), Gülhane Military Medical School, Ankara, Turkey; the Department of Radiology (V.A.), Gölcük Military Hospital, Kocaeli, Turkey.

Diffusion-weighted magnetic resonance imaging (MRI) can be used to visualize the arbitrary movement of water molecules (Brownian motion) that causes phase dispersion and consequential signal loss (1). Because diffusion-weighted imaging (DWI) provides both qualitative and quantitative information without a considerable increase in the study time and does not require intravenous contrast media, it has been added into routine imaging protocols. By using recent technologic advances such as echo-planar imaging, high-gradient amplitudes, multichannel coils, and parallel imaging, its applications have extended beyond neurological applications (2, 3). The aims of this pictorial essay were to outline the biological basis and the imaging technique of DWI and to review the pediatric extracranial applications of DWI, including tissue characterization, organ functionality assessment, and tumor treatment monitoring.

The biological basis and imaging technique of DWI

DWI measures the random motion of water molecules in tissue. When an MRI sequence is expanded with a diffusion-sensitizing gradient scheme, the sequence can be made sensitive to the diffusion (2, 3). Thus, both the mobility and viscosity of water molecules can be assessed, and the water balance between intracellular and extracellular compartments can be determined (1). Diffusion can be measured using two complementary dephasing-rephasing gradients, which are added to a spin-echo T2-weighted sequence. The dephasing gradient causes the spinning protons to fall out of phase with one another, and then the rephasing gradient rephases the protons completely with one another but only if there has been no movement of the water molecules between the applications of the two diffusion gradients. When there is movement of water, the protons are not brought back completely into phase by the second diffusion gradient. The degree of water motion has been found to be proportional to the degree of signal attenuation: the greater the displacement of the spins, the greater the signal loss (3). In contrast, in the case of reduction in diffusivity, static water molecules acquire phase information from the first dephasing gradient, but the information will be rephased by the second rephasing gradient without a significant change in the measured signal intensity (3–5).

The diffusion weighting of the sequence is defined by the factor b (s/mm^2). Factor b is calculated with the following formula, which includes the duration of the diffusion gradients (λ), power of the gradient (G), time interval between gradients (Δ), and gyromagnetic constant (γ): b=γ^2G$^2\lambda^2$(Δ-λ/3) (1–3). The sensitivity of the DWI sequence to water motion can be varied by changing the gradient amplitude, the duration of the applied gradient, and the time interval between the paired gradients. On clinical MRI scanners, the diffusion sensitivity can easily be altered
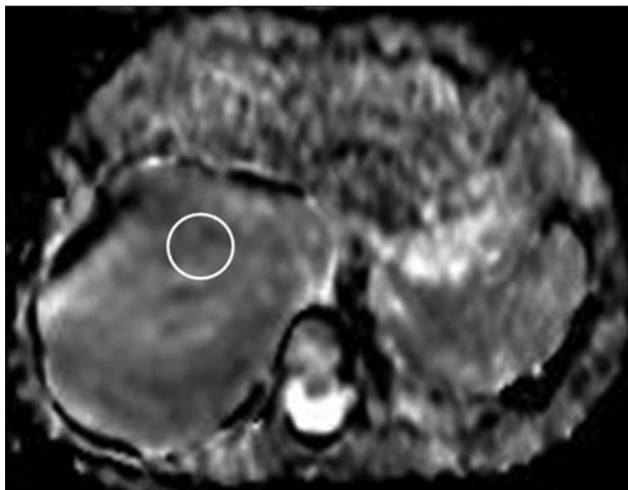
Figure 1. An axial apparent diffusion coefficient (ADC) map of a five-year-old female with thoracic ganglioneuroma. The ADC value is 1.20×10^{-3} mm^2/s.
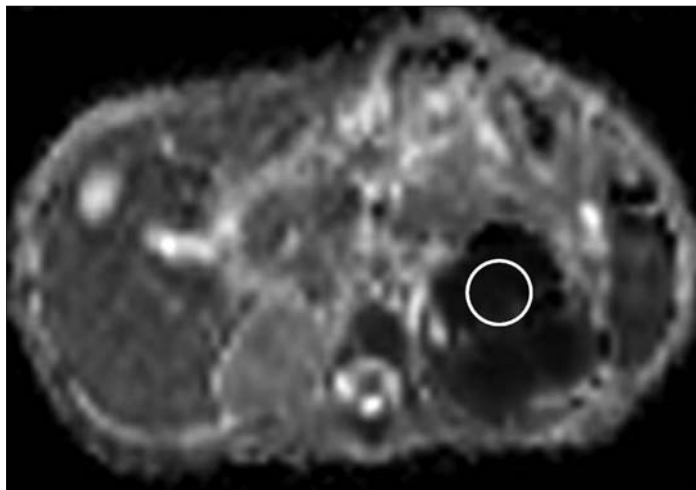

Figure 2. An axial ADC map of a 13-month-old female with neuroblastoma of the left adrenal gland. The ADC value is 0.72×10^{-3} mm^2/s.

by changing the parameter known as the b value, which is proportional to these three factors. When the b value is changed, it is usually the gradient amplitude, rather than the duration or time interval between gradients, that is altered (3).

The cellularity and capillary perfusion (pseudo-diffusion), temperature, diffusivity, b value, macroscopic motion and T2-weighted intensity are the factors that affect the signal intensities on DWIs with low and high b values and the corresponding apparent diffusion coefficient (ADC) maps. Therefore, the overall signal intensity on DWI reflects the diffusion conspicuity, the spin density, and T2 value of the image voxels (1–6). The amount of diffusion is determined by the diffusion coefficient. Because the in vivo measurement of the diffusion coefficient is affected by several factors, the term "apparent diffusion coefficient" rather than "diffusion coefficient" is used in clinical practice (5–7).

The ADC is calculated for each pixel of the image and is displayed as a parametric map. By drawing regions of interest, ADCs of different tissues can be measured. In clinical applications, DWI is usually performed using two or more b values. One of the b values is a high b value (usually 800 to 1000 s/mm^2), while the rest of the b values are low b values ($\leq$100 s/mm^2). By using more b values, the errors in the calculation of the ADC maps can be diminished, and accuracy can be increased (1, 2, 4–6). The ADC value is calculated by using two images with high and low b values,

according to the following equation: ADC=-[ln (SI_h/SI_l)]/(b_h-b_l), where SI_h and SI_l are the signal intensities in the region of interest obtained with two motion-probing gradients (b_h and b_l, respectively) (1–4). The areas of restricted diffusion are demonstrated by low intensity areas on ADC maps, contrary to increased diffusion areas, which appear as high-intensity areas. Tissue characterization can be performed by comparing signal-intensity attenuation, which depends on the variation in molecular diffusion on images acquired using different b values (8).

In ADC maps that are performed with low b values, aside from true diffusion, perfusion of the tissue (pseudo-diffusion) is also prominent. The perfusion effect is significantly reduced by increasing the b value. The ADC maps formed by using high b values are also useful in lesion characterization. However, by using high b values, the signal-to-noise ratio (SNR) of the image is reduced, and sensitivity to magnetic susceptibility, motion, and eddy current artifacts increases (1, 2, 6).

Because the signal is generated by a spin-echo pulse sequence, the overall signal intensity on DWI reflects the diffusion conspicuity, the spin density and T2 value of the imaged voxels. T2 signal elongation increases signal intensities in DWI. This effect is known T2 shine-through and decreases when the b value increases (1).

Poor ADC reproducibility and low image quality due to poor SNR, limited spatial resolution, and echo-planar imaging-related artifacts (especially those

acquired with high b values and primarily distortion, ghosting, blurring, and eddy currents) are the main limitations of DWI (1, 3, 6).

ADC depends on the imaging equipment, observer, and biologic factors. Accurate understanding of ADC measurement reproducibility and inter-imager variability is a critical issue for the application of quantitative ADC measurements for disease characterization and tumor response assessment. Image acquisition schemes for MRI systems from different vendors may vary and cause variability in ADC measurements. To compare the results from different MRI equipment and centers, the standardization of imaging parameters is needed to minimize the measurement variability across platforms and to facilitate multicenter studies (3, 6).

DWI interpretation

There is a negative correlation between ADC values and the cellularity, extracellular tortuosity, and nucleus/cytoplasm ratio of extra-cranial tumors in children (1–3, 9–13). It has been shown that the ADC values of malignant masses are relatively lower than the ADC values of benign masses (Figs. 1 and 2) (9–14). Recent studies reported that malignant and benign lesions can be discriminated with high accuracy by visual assessment of the diffusion trace images and ADC maps (6, 9, 15). Malignant pathologies in DWI appear as a high signal, which persists at high b values and correlates with low ADC values in ADC maps due to restricted diffusion (Figs. 3 and 4). Most of the
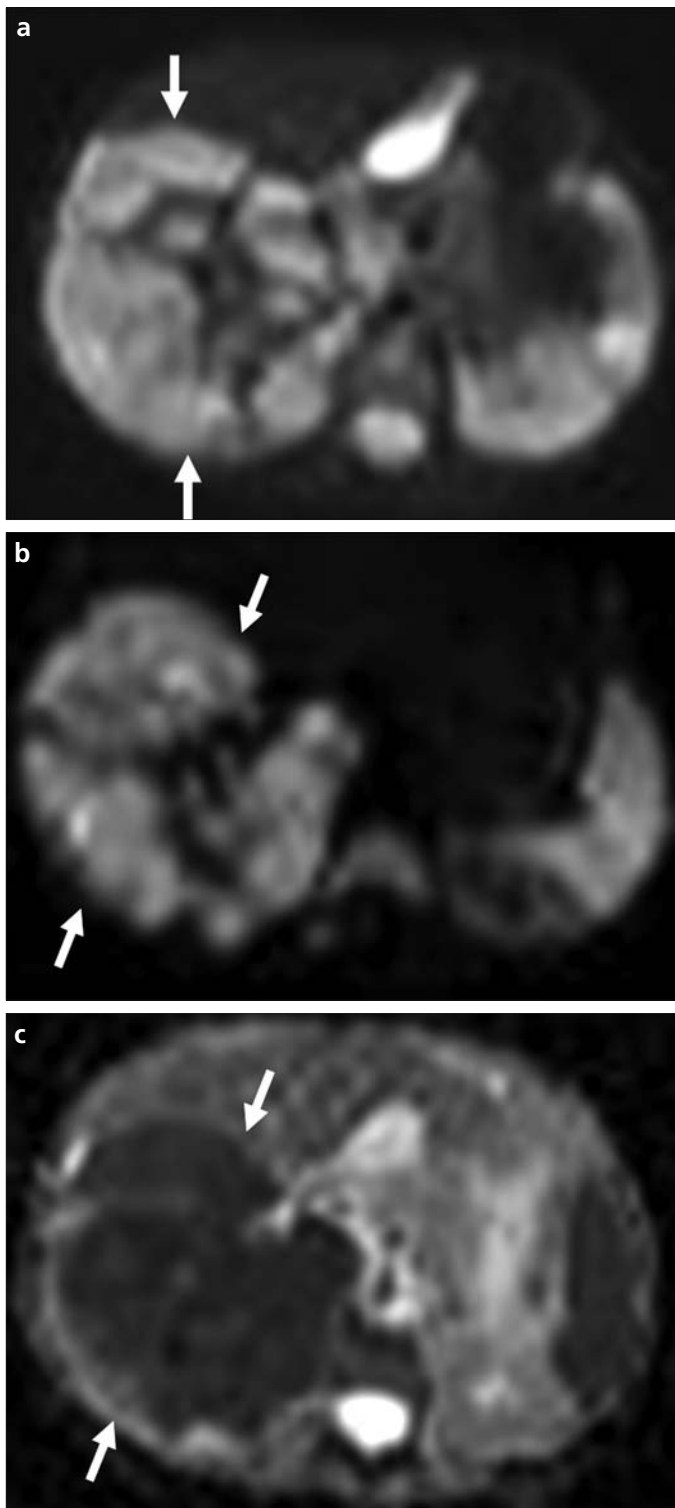
Figure 3. a–c. Right-sided adrenal gland neuroblastoma in a seven-year-old female. An axial diffusion-weighted (DW) image at the level of the upper abdomen obtained using a b value of 0 s/mm^2 shows a hyperintense mass (**a**, *arrows*). An axial DW image obtained using a b value of 800 s/mm^2 confirms the hyperintense mass *(arrows)* with slight signal attenuation when compared with Fig. 3a **(b)**. The ADC map shows a low ADC value (0.74×10^{-3} mm^2/s) suggesting restricted diffusion **(c**, *arrows*).
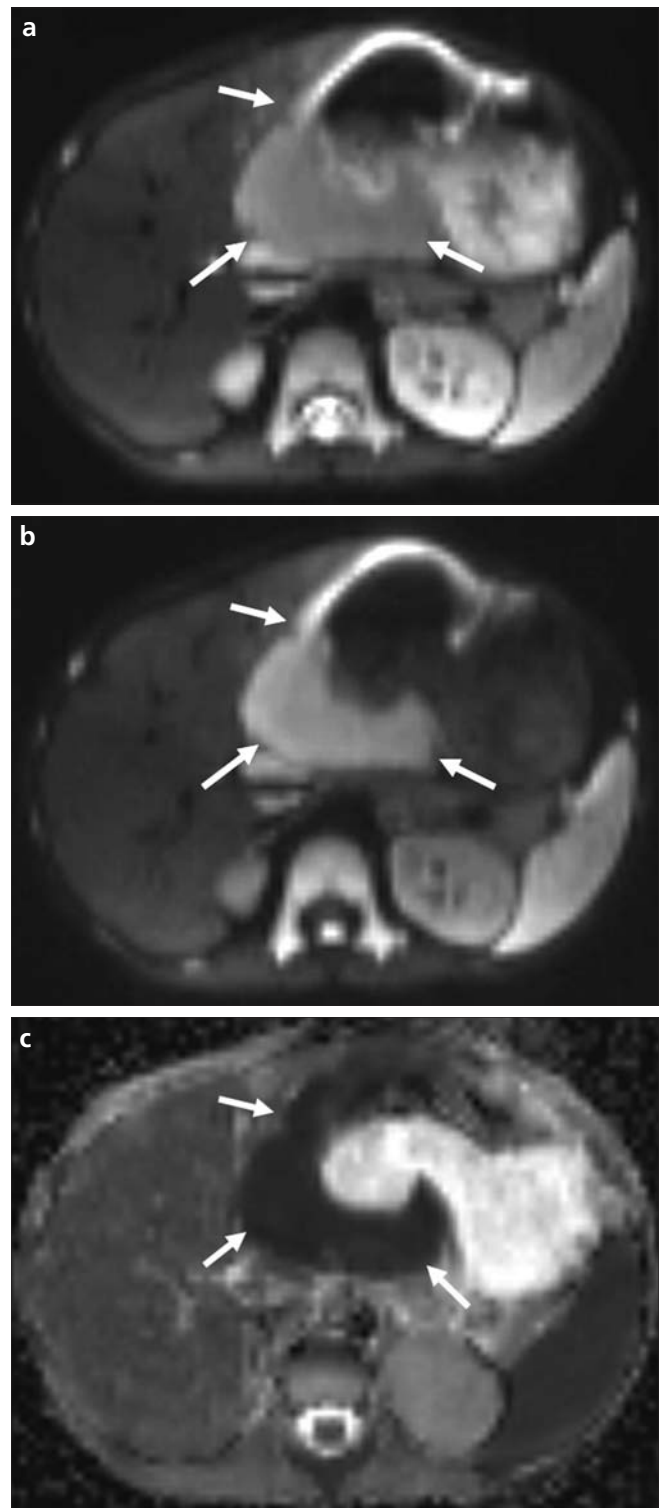
Figure 4. a–c. Gastric lymphoma in a six-year-old male. An axial DW image at the level of the upper abdomen obtained using a b value of 0 s/mm^2 shows a hyperintense antral mass (**a**, *arrows*). An axial DW image obtained using a b value of 800 s/mm^2 confirms the hyperintense mass *(arrows)* with no prominent signal difference when compared with Fig. 4a **(b)**. ADC map shows a low ADC value (0.43×10^{-3} mm^2/s) within the mass, which is consistent with restricted diffusion **(c**, *arrows*).

benign pathologies in DWI appear as high signal at low b values, which is fully suppressed at high b values and correlates with areas of high ADC values in ADC maps (T2 shine-through effect) that demonstrate increased diffusion. Cystic or necrotic portions of the tumor show greater signal attenuation on high b value images and correlate with areas of high ADC values in ADC maps. More cellular solid tumor regions continue to show a relatively high signal on high b value images and correlate with low ADC values in ADC maps (Fig. 5) (1–3, 5–7, 9, 15, 16). However, abscesses are also characterized by similar signal intensity and ADC values as those associated with malignancies due to its viscous content (9, 15).

In heterogeneous lesions with both low- and high-intensity areas on ADC maps, ADC measurements can be challenging. In these lesions, one should assess the ADC value in the component with the lowest intensity or separately assess the areas with low or high intensities. However, the measurement of ADC values with large regions-of-interest covering both low- and high-intensity areas can cause misinterpretation. In these equivocal cases, aside from DWI, using conventional and contrast-enhanced images may be helpful for lesion characterization (13, 15).

It is important to remember that ADC maps and high b value images should never be interpreted separately. It is imperative to emphasize the importance of the interpretation of DWI with the anatomic images to avoid the pitfalls, which are many. There may be overlaps between ADC values of the malignant and benign pathologies. Furthermore, normal tissues including peripheral nerves, normal lymph nodes, normal endometrium, and bowel can show low ADC values. Areas of fibrosis also show low ADC values (1–3, 7, 9, 11–15). DWI still has a limited role in the detection and characterization of small-sized lesions less than 1 cm because of the limited spatial resolution and artifacts such as susceptibility, ghosting, blurring, and eddy currents (3, 9, 15).

Extra-neurological applications of DWI
Tissue characterization

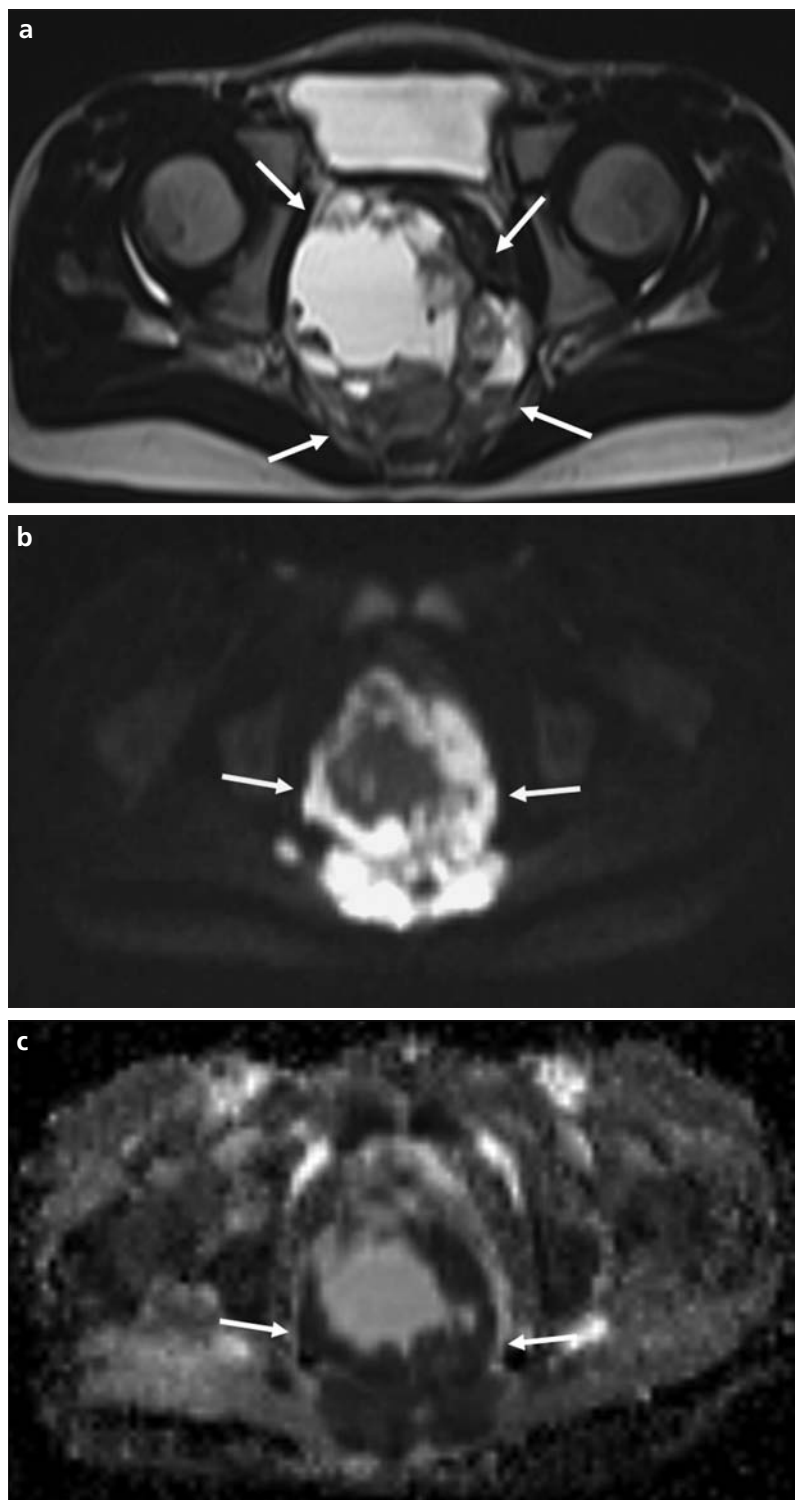Although, statistically significant differences in ADC values between the

Figure 5. a–c. An undifferentiated presacral germ cell tumor in a six-year-old female. An axial T2-weighted image at the level of the lower pelvis shows a presacral mass *(arrows)* with a hyperintense central necrotic area surrounded by a heterogeneous hypointense peripheral solid component **(a)**. An axial DW image acquired using a b value of 800 s/mm^2 through the pelvic floor reveals that the peripheral solid components of the mass *(arrows)* exhibit a high signal, while the central necrotic portion shows significant signal attenuation **(b)**. The ADC map demonstrates a low ADC (0.68×10^{-3} mm^2/s) in the peripheral rim *(arrows)* and a high ADC value (2.21×10^{-3} mm^2/s) within the necrotic core, which is consistent with restricted and increased diffusion, respectively **(c)**.

benign and malignant pediatric extracranial tumors have been shown, ADC value overlaps of some malignant and benign lesions have also been reported (Figs. 6–9) (9–14). Also, in pediatric patients, Humphries et al. (16) found relatively low ADC values in malignant masses (mean, 1.00×10^{-3} mm^2/s) and relatively high ADC values in benign masses (mean, 1.35×10^{-3} mm^2/s). In this study, benign masses were unable to be differentiated from malignant masses using ADC values. In malignant tumors, reduced ADC values are thought to be due to cellular membranes impeding the mobility of water protons. Necrotic tissues, on the other hand, show high ADC values that result from larger diffusion areas

as a consequence of the loss of membrane integrity (6, 9, 11).

Inflammation also reduces ADC values (1–3). In the inflamed tissue, the decreased ADC value is considered to be the result of the increased number and size of cells (Fig. 10). ADC has been used to distinguish abscesses, which have low ADC values due to high viscosity and cellularity in the abscess cavity, from cystic and necrotic metastases with higher ADC values (3). On visual assessment, the central content of the abscess is markedly hyperintense on low and high b value DWIs and hypointense on ADC maps as compared with the normal parts of the tissue, whereas the cystic-necrotic contents of the tumors and cystic masses

are hyperintense on low b value DWIs, markedly hypointense on high b value DWIs and hyperintense on ADC maps (Fig. 11) (15).

Significant statistical differences between the ADC values of benign and malignant lymph nodes have been reported (17–20). In general, lower ADC values were measured in the malignant lymph nodes (metastatic or lymphomatous) compared with benign ones, with variations in ADC values according to the identity of the primary tumor (Fig. 12) (18). However, in some studies, overlaps in ADC values of the malignant and benign lymph nodes were reported (18, 20, 21). Muenzel et al. (21) reported that lympadenopathy caused by *Bartonella henselae* infection
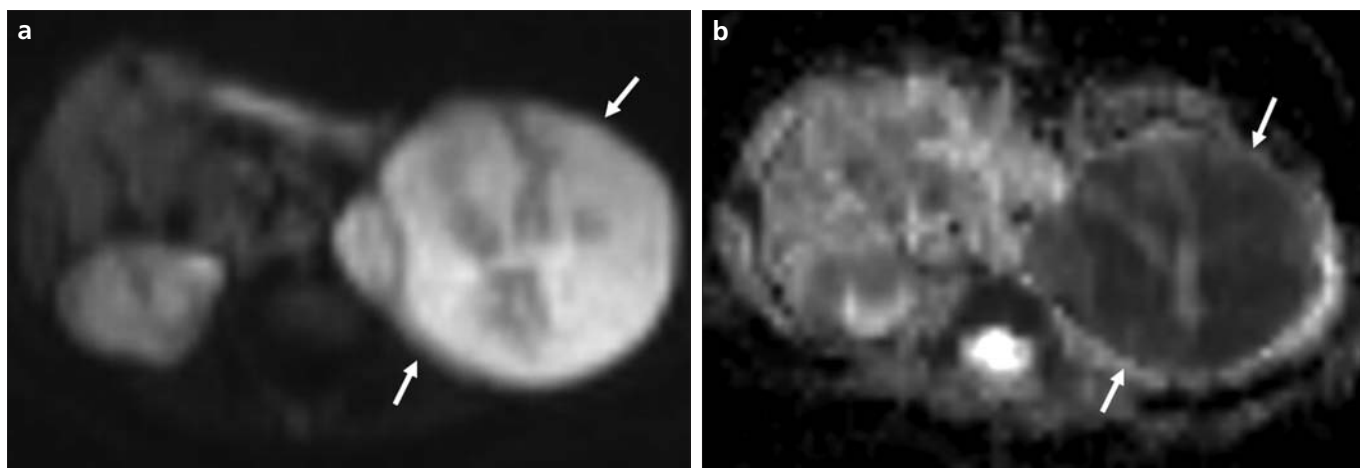

Figure 6. a, b. Wilms' tumor in a six-year-old male. An axial DW image obtained using a b value of 800 s/mm^2 shows a high-signal, left renal mass (**a**, *arrows*). The ADC map demonstrates a low ADC value (0.73×10^{-3} mm^2/s) within the lesion *(arrows)*, suggesting restricted diffusion (**b**).
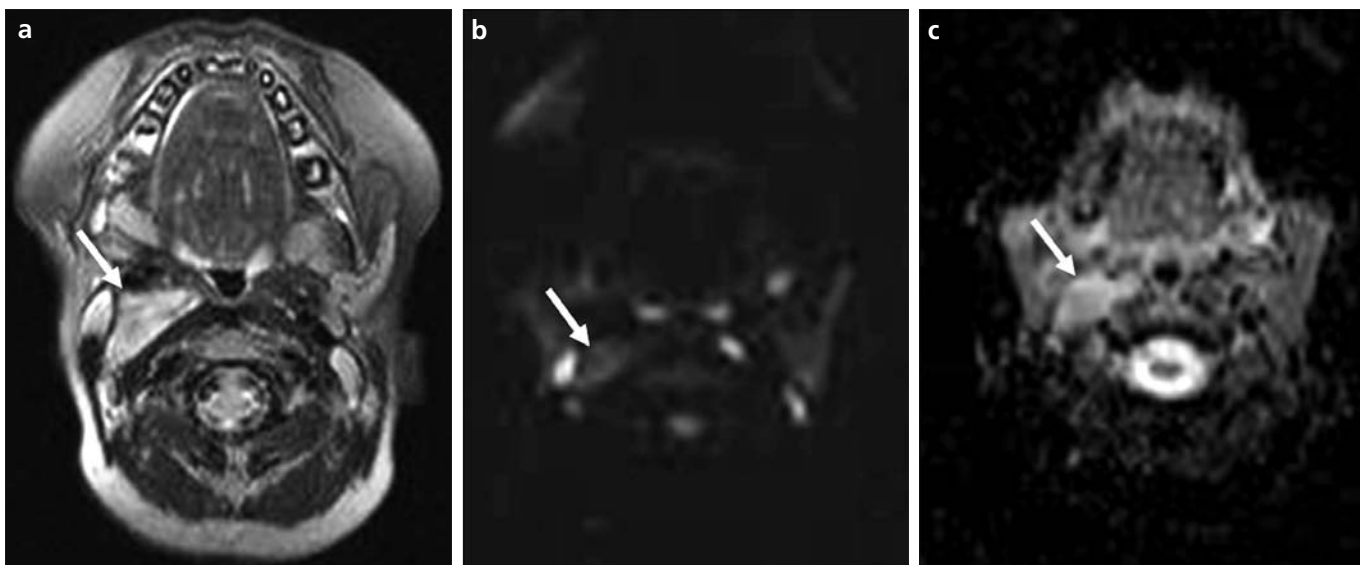

Figure 7. a–c. Cervical ganglioneuroma in an eight-year-old male. An axial T2-weighted MR image through the oropharynx shows a hyperintense paravertebral mass (**a**, *arrows*). A DW image obtained using a b value of 800 s/mm^2 demonstrates a slightly hyperintense lesion (**b**, *arrows*). The corresponding ADC map shows a slightly high ADC value (1.25×10^{-3} mm^2/s) within the mass (**c**, *arrows*).
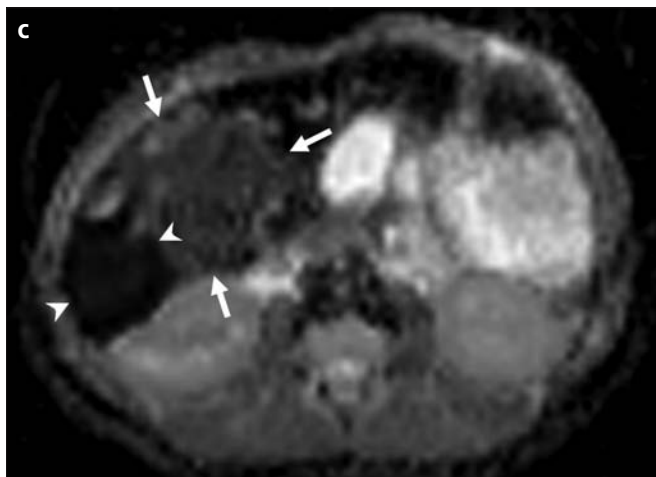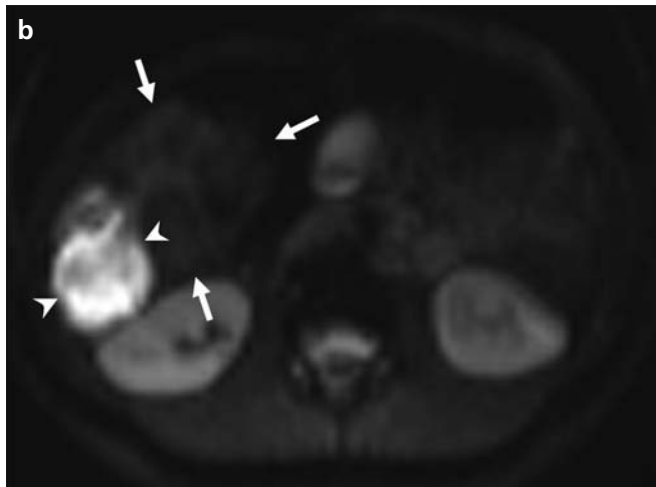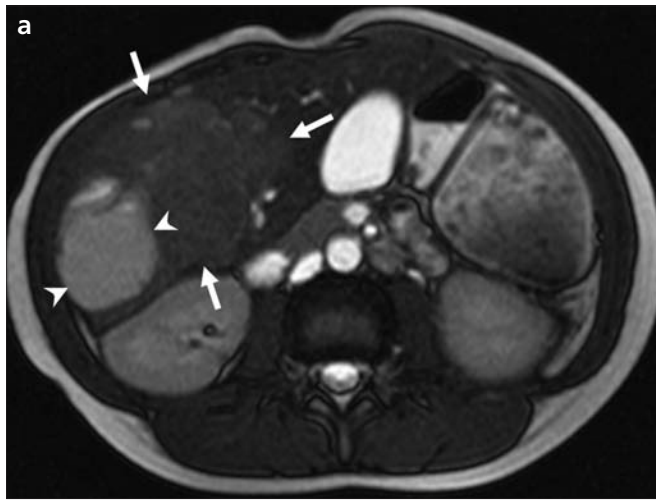
Figure 8. a–c. Peliosis hepatis, which is a benign lesion consisting of multiple blood-filled lacunar spaces within the liver, mimicking a diffusion-restricting malignant lesion in a 10-year-old male. An axial T2-weighted image shows a mixed signal-intensity lesion *(arrows and arrowheads)* in the right lobe of the liver **(a)**. An axial DW image acquired using a b value of 800 s/mm² reveals a mass with slightly high-signal areas **(b,** *arrows***)** and a focal area showing marked hyperintensity **(b,** *arrowheads***)**. The ADC map demonstrates a low ADC (0.72×10^{-3} mm²/s) in a focal area **(c,** *arrowheads***)** that is markedly hyperintense on b-800 images and displays a relatively high ADC value (1.49×10^{-3} mm²/s) within the other areas, which is consistent with restricted and increased diffusion, respectively **(c,** *arrows***)**. Low and high ADC values may be related with old and new blood products within the lesion.
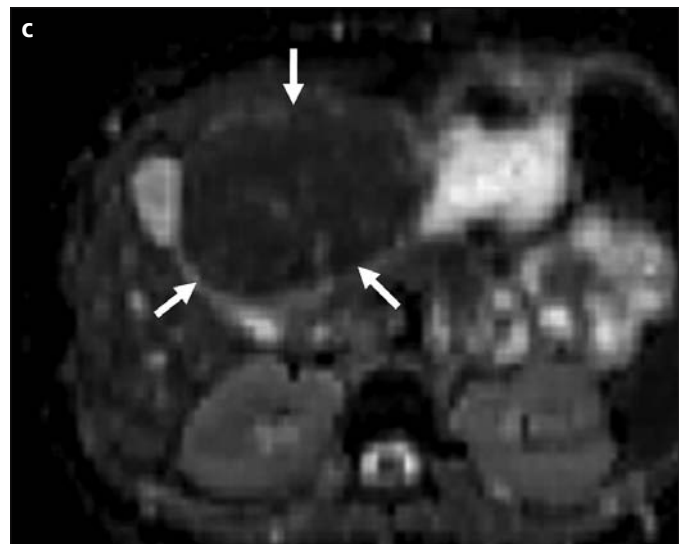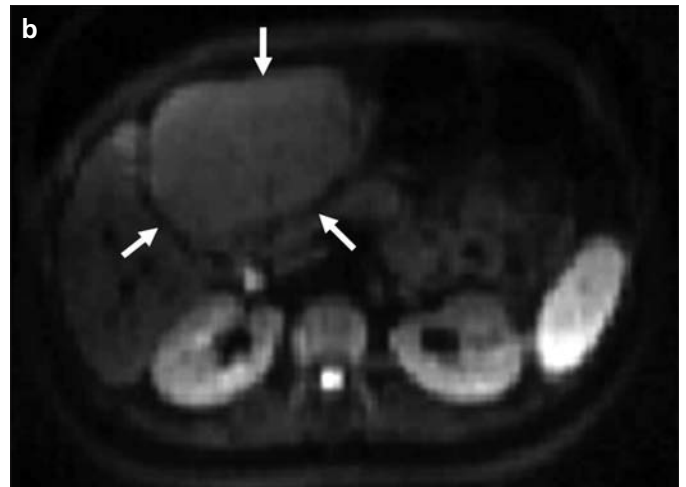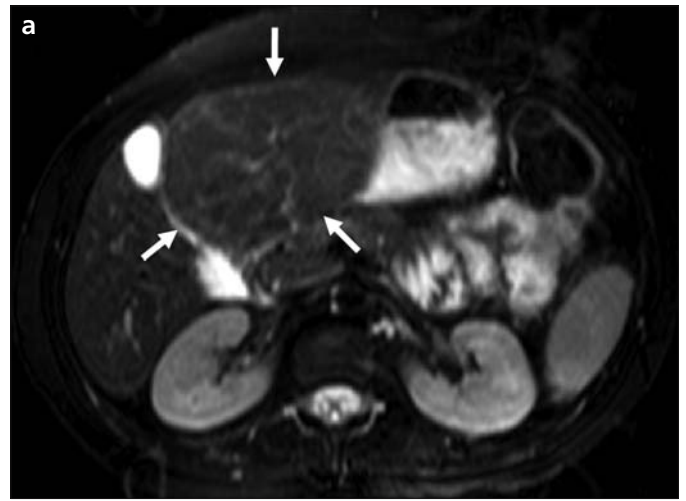

Figure 9. a–c. Focal nodular hyperplasia presenting as an equivocal lesion in a 15-year-old female. An axial fat saturation T2-weighted image shows an isointense focal liver lesion **(a,** *arrows***)**. An axial DW image acquired using a b value of 800 s/mm² reveals mild hyperintensity within the lesion **(b,** *arrows***)**. The ADC map demonstrates a relatively low ADC value (1.21×10^{-3} mm²/s) within the lesion **(c,** *arrows***)**.
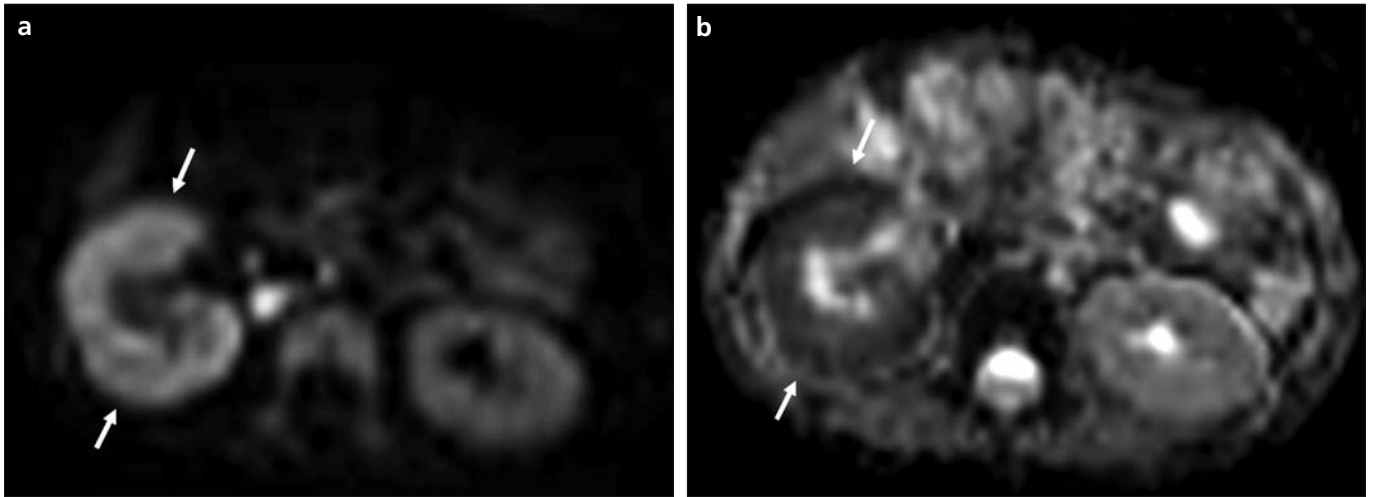
Figure 10. a, b. Pyelonephritis in a three-year-old female. An axial DW image obtained using a b value of 800 s/mm² at the level of the renal hilum demonstrates an increased signal in the right renal parenchyma (**a**, *arrows*). The corresponding ADC map demonstrates low ADC values (0.87×10⁻³ mm²/s) in the parenchyma, which is consistent with restricted diffusion (**b**, *arrows*).
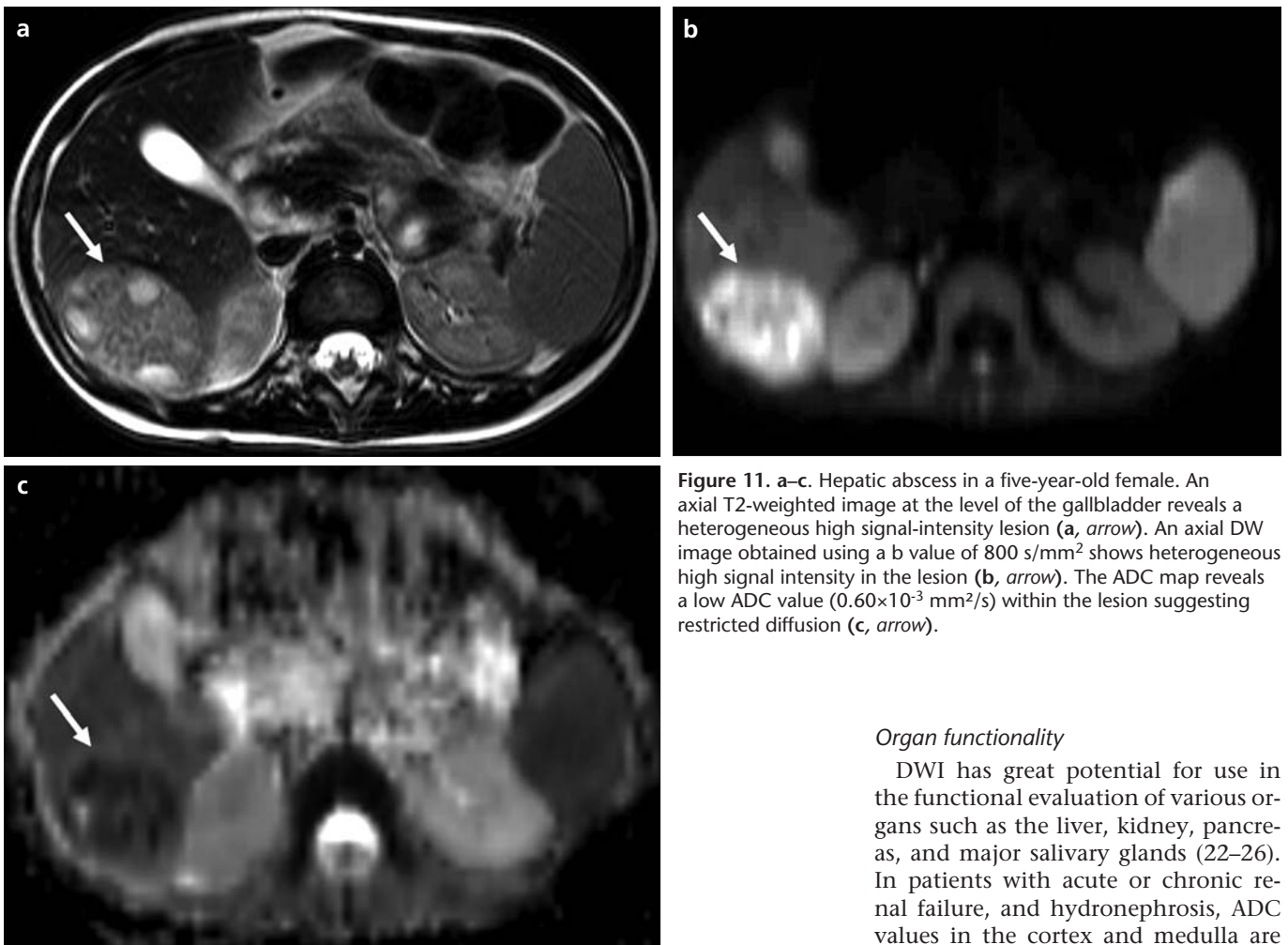

Figure 11. a–c. Hepatic abscess in a five-year-old female. An axial T2-weighted image at the level of the gallbladder reveals a heterogeneous high signal-intensity lesion (**a**, *arrow*). An axial DW image obtained using a b value of 800 s/mm² shows heterogeneous high signal intensity in the lesion (**b**, *arrow*). The ADC map reveals a low ADC value (0.60×10⁻³ mm²/s) within the lesion suggesting restricted diffusion (**c**, *arrow*).

yields low ADC values in diffusion-weighted MRI, as is typically seen in malignant disease. Also, the reported cut-off values for discriminating malignant and benign lymphadenopathies show differences according to the underlying cause and localization of the lymph nodes.

Organ functionality

DWI has great potential for use in the functional evaluation of various organs such as the liver, kidney, pancreas, and major salivary glands (22–26). In patients with acute or chronic renal failure, and hydronephrosis, ADC values in the cortex and medulla are significantly lower than those of the normal kidneys. In these patients, a positive correlation between the ADCs and glomerular filtration rate has been described (Fig. 13) (22–24).

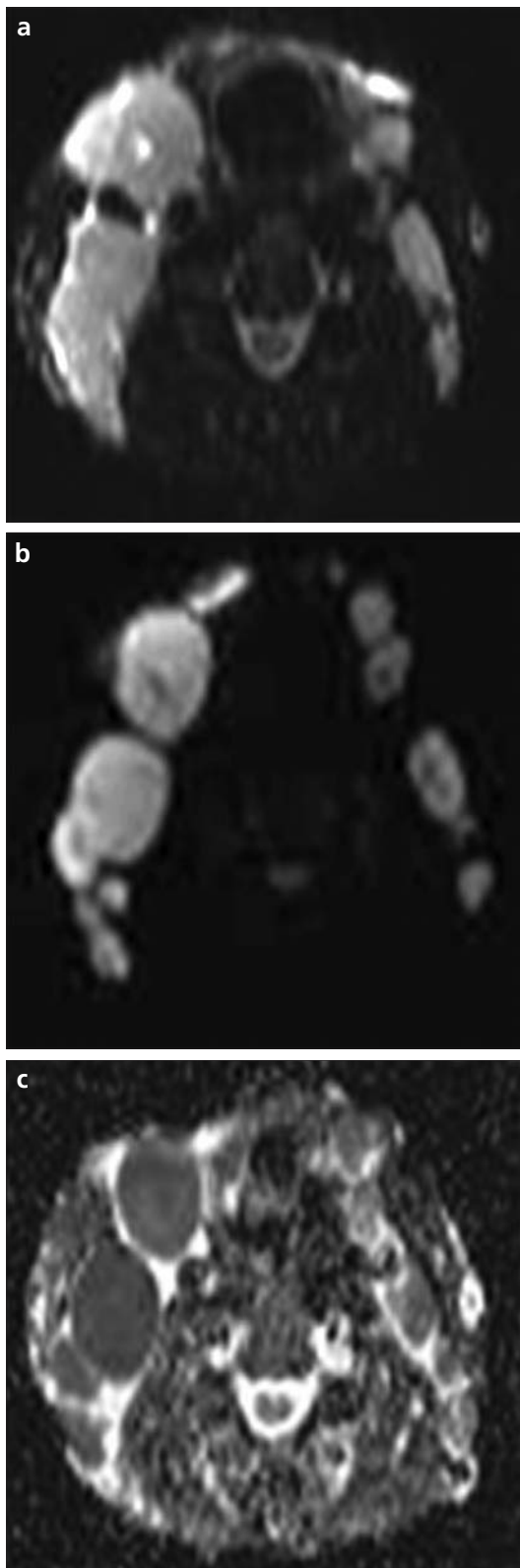DWI can also detect acute pancreatitis with reduced ADC values at the time

Figure 12. a–c. Non-Hodgkin's lymphoma in a 10-year-old male. An axial DW image at the level of the upper neck acquired using a b value of 0 s/mm² shows hyperintense lymph nodes **(a)**. An axial DW image obtained using a b value of 800 s/mm² confirms the presence of a hyperintense mass with slight signal attenuation **(b)**. The ADC map shows a low ADC value (0.65×10^{-3} mm²/s) within the lesion suggesting restricted diffusion **(c)**.
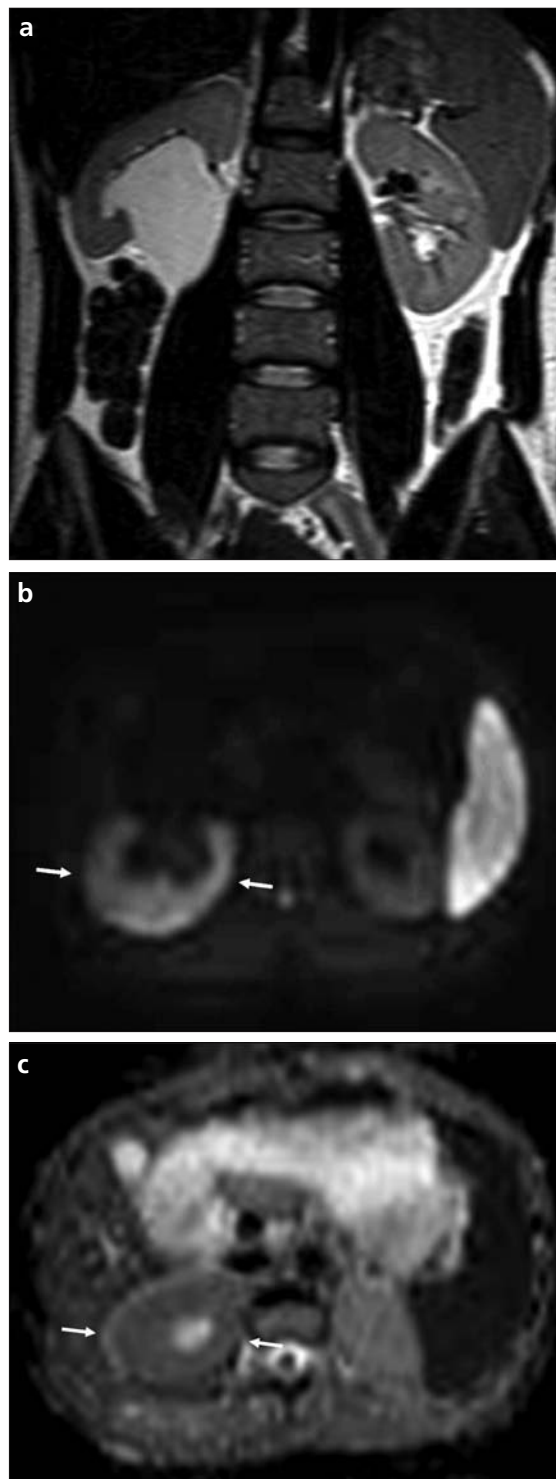
Figure 13. a–c. Right hydronephrosis due to ureteropelvic junction stenosis in a four-year-old male. A coronal T2-weighted turbo spin-echo MR image shows the dilated right renal pelvis without ureteral dilation **(a)**. An axial DW image obtained using a b value of 800 s/mm² demonstrates an increased signal in the right renal parenchyma **(b,** *arrows***)**. The corresponding ADC map demonstrates low ADC values (0.93×10^{-3} mm²/s) in the renal parenchyma, which is consistent with restricted diffusion due to impaired renal function **(c,** *arrows***)**. Impaired right renal function was proved with renal scintigraphy using 99mTc-DTPA.

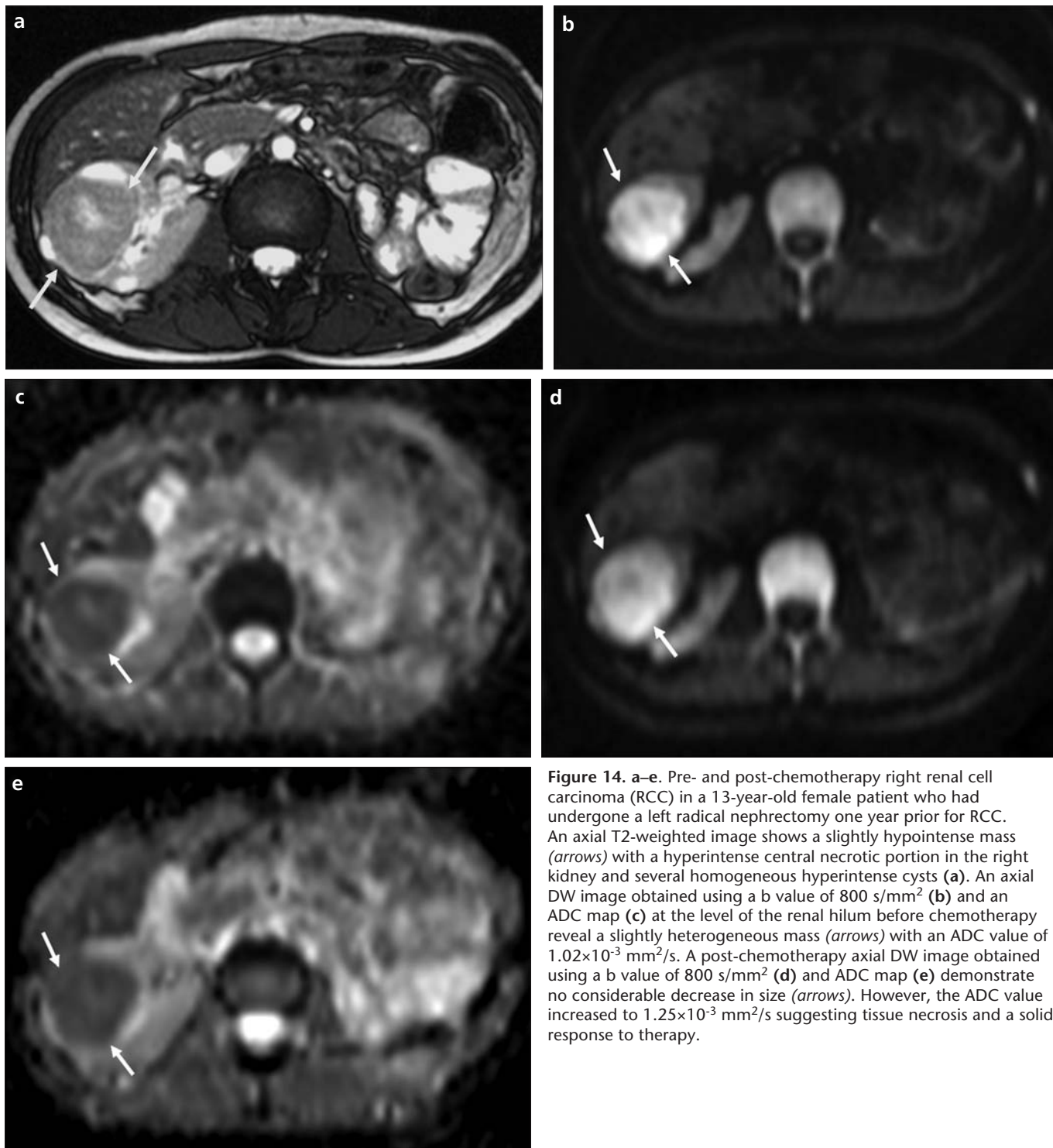**Figure 14. a–e.** Pre- and post-chemotherapy right renal cell carcinoma (RCC) in a 13-year-old female patient who had undergone a left radical nephrectomy one year prior for RCC. An axial T2-weighted image shows a slightly hypointense mass *(arrows)* with a hyperintense central necrotic portion in the right kidney and several homogeneous hyperintense cysts **(a)**. An axial DW image obtained using a b value of 800 s/mm^2 **(b)** and an ADC map **(c)** at the level of the renal hilum before chemotherapy reveal a slightly heterogeneous mass *(arrows)* with an ADC value of 1.02×10^{-3} mm^2/s. A post-chemotherapy axial DW image obtained using a b value of 800 s/mm^2 **(d)** and ADC map **(e)** demonstrate no considerable decrease in size *(arrows)*. However, the ADC value increased to 1.25×10^{-3} mm^2/s suggesting tissue necrosis and a solid response to therapy.

of diagnosis (25). The ADC values of cirrhotic livers are significantly lower than those of normal livers due to fibrosis and inflammation (26).

Predicting and monitoring treatment response

DWI has been suggested as the modality of choice for the early detection of treatment response in tumors (16, 27–29). Reduction in tumor volume is considered to be a relatively late finding in association with the response to chemotherapy or radiotherapy. However, DWI with the calculation of ADC has been suggested as an early marker of the therapy response in tumors because it is assumed that less restricted diffusion is associated with decreased cellularity of the tumor (Fig. 14) (28). McDonald et al. (28) reported that the ADC changes during chemotherapy in childhood abdominal tumors were measurable. They noted that distinct patterns of shift could be observed. ADC change was therefore promising as a non-invasive biomarker

for therapy response. Also, according to the studies performed in adult groups, ADC measurements often appear to be capable of predicting the tumor response to chemotherapy and radiation treatment (2, 3, 30). The response to chemotherapy or radiation treatment in cellular tumors with low pre-treatment ADC values is better than those of tumors with higher pre-treatment ADC values (30). Further studies focusing on this subject in pediatric malignancies are needed.

Conclusion

DWI with an ADC map is a new promising technique that can be useful for lesion characterization and assessment of the tumor response to treatment in children with extra-neurological pathologies. This technique does not require intravenous contrast media and can be performed within several minutes. However, there are some limitations, e.g., ADC value overlaps in some malignant and benign lesions, low SNR, the difficulty in the assessment of relatively small lesions, and motion artifacts. The addition of DWI into routine MRI protocols can provide supplementary physiological and functional information for conventional and contrast-enhanced MRI sequences in pediatric patients.

Conflict of interest disclosure

The authors declared no conflict of interest.

References

1. Colagrande S, Belli G, Politi LS, Mannelli L, Pasquinelli F, Villari N. The influence of diffusion- and relaxation-related factors on signal intensity: an introductive guide to magnetic resonance diffusion-weighted imaging studies. J Comput Assist Tomogr 2008; 32:463–474.
2. Thoeny HC, De Keyzer F. Extracranial applications of diffusion-weighted magnetic resonance imaging. Eur Radiol 2007; 17:1385–1393.
3. Koh DM, Collins DJ. Diffusion-weighted MRI in the body: applications and challenges in oncology. AJR Am J Roentgenol 2007; 188:1622–1635.
4. Stejskal EO, Tanner JE. Spin diffusion measurements: spin echoes in the presence in the presence of a time-dependent field gradient. J Chem Phys 1965; 42:288–292.
5. Le Bihan D, Breton E, Lallemand D, Grenier P, Cabanis E, Laval-Jeantet M. MR imaging of intravoxel incoherent motions: application to diffusion and perfusion in neurologic disorders. Radiology 1986; 161:401–407.
6. Taouli B, Koh DM. Diffusion-weighted MR imaging of the liver. Radiology 2010; 254:47–66.
7. Demir OI, Obuz F, Sağol O, Dicle O. Contribution of diffusion-weighted MRI to the differential diagnosis of hepatic masses. Diagn Interv Radiol 2007; 13:81–86.
8. Herneth AM, Guccione S, Bednarski M. Apparent diffusion coefficient: a quantitative parameter for in vivo tumor characterization. Eur J Radiol 2003; 45:208–213.
9. Kocaoglu M, Bulakbasi N, Sanal HT, et al. Pediatric abdominal masses: diagnostic accuracy of diffusion weighted MRI. Magn Reson Imaging 2010; 28:629–636.
10. MacKenzie JD, Gonzalez L, Hernandez A, Ruppert K, Jaramillo D. Diffusion-weighted and diffusion tensor imaging for pediatric musculoskeletal disorders. Pediatr Radiol 2007; 37:781–788.
11. Abdel Razek AA, Gaballa G, Elhawarey G, Elshafey M, Elhadedy T. Characterization of pediatric head and neck masses with diffusion-weighted MR imaging. Eur Radiol 2009; 19:201–208.
12. Alibek S, Cavallaro A, Aplas A, Uder M, Staatz G. Diffusion weighted imaging of pediatric and adolescent malignancies with regard to detection and delineation: initial experience. Acad Radiol 2009; 16:866–871.
13. Abdel Razek AA, Soliman N, Elashery R. Apparent diffusion coefficient values of mediastinal masses in children. Eur J Radiol 2011 Mar 24. [Epub ahead of print]
14. Battal B, Kocaoglu M, Atay AA, Bulakbasi N. Multifocal peliosis hepatis: MR and diffusion-weighted MR-imaging findings of an atypical case. Ups J Med Sci 2010; 115:153–156.
15. Battal B, Kocaoglu M, Akgun V, et al. Diffusion-weighted imaging in the characterization of focal liver lesions: efficacy of visual assessment. J Comput Assist Tomogr 2011; 35:326–331.
16. Humphries PD, Sebire NJ, Siegel MJ, Olsen ØE. Tumors in pediatric patients at diffusion-weighted MR imaging: apparent diffusion coefficient and tumor cellularity. Radiology 2007; 245:848–854.
17. Thoeny HC. Diffusion-weighted MRI in head and neck radiology: applications in oncology. Cancer Imaging 2011; 10:209–214.
18. Holzapfel K, Duetsch S, Fauser C, Eiber M, Rummeny EJ, Gaa J. Value of diffusion-weighted MR imaging in the differentiation between benign and malignant cervical lymph nodes. Eur J Radiol 2009; 72:381–387.
19. Akduman EI, Momtahen AJ, Balci NC, Mahajann N, Havlioglu N, Wolverson MK. Comparison between malignant and benign abdominal lymph nodes on diffusion-weighted imaging. Acad Radiol 2008; 15:641–646.
20. Abdel Razek AA, Soliman NY, Elkhamary S, Alsharaway MK, Tawfik A. Role of diffusion-weighted MR imaging in cervical lymphadenopathy. Eur Radiol 2006; 16:1468–1477.
21. Muenzel D, Duetsch S, Fauser C, et al. Diffusion-weighted magnetic resonance imaging in cervical lymphadenopathy: report of three cases of patients with Bartonella henselae infection mimicking malignant disease. Acta Radiol 2009; 50:914–916.
22. Thoeny HC, De Keyzer F, Oyen RH, Peeters RR. Diffusion-weighted MR imaging of kidneys in healthy volunteers and patients with parenchymal diseases: initial experience. Radiology 2005; 235:911–917.
23. Toyoshima S, Noguchi K, Seto H, Shimizu M, Watanabe N. Functional evaluation of hydronephrosis by diffusion-weighted MR imaging. Relationship between apparent diffusion coefficient and split glomerular filtration rate. Acta Radiol 2000; 41:642–646.
24. Xu Y, Wang X, Jiang X. Relationship between the renal apparent diffusion coefficient and glomerular filtration rate: preliminary experience. J Magn Reson Imaging 2007; 26:678–681.
25. Shinya S, Sasaki T, Nakagawa Y, Guiquing Z, Yamamoto F, Yamashita Y. Acute pancreatitis successfully diagnosed by diffusion-weighted imaging: a case report. World J Gastroenterol 2008; 14:5478–5480.
26. Taouli B, Tolia AJ, Losada M, et al. Diffusion weighted MRI for quantification of liver fibrosis: preliminary experience. AJR Am J Roentgenol 2007; 189:799–806.
27. Chenevert TL, Stegman LD, Taylor JM, et al. Diffusion magnetic resonance imaging: an early surrogate marker of therapeutic efficacy in brain tumors. J Natl Cancer Inst 2000; 92:2029–2036.
28. McDonald K, Sebire NJ, Anderson J, Olsen OE. Patterns of shift in ADC distributions in abdominal tumours during chemotherapy-feasibility study. Pediatr Radiol 2011; 41:99–106.
29. Voss SD. Pediatric oncology and the future of oncological imaging. Pediatr Radiol 2011; 41:172–185.
30. Thoeny HC, Ross BD. Predicting and monitoring cancer treatment response with diffusion-weighted MRI. J Magn Reson Imaging 2010; 32:2–16.